Journal of ELECTRONIC MATERIALS, Vol. 45, No. 1, 2016
DOI: 10.1007/s11664-015-4166-x

Enhanced Photoelectrochemical Performance of TiO_2 Nanorod Arrays by a 500°C Annealing in Air: Insights into the Mechanism

SHUANG ZHANG,[1] XIUQUAN GU,[1,2] YULONG ZHAO,[1] and YINGHUAI QIANG[1]

1.—School of Materials Science and Engineering, China University of Mining and Technology, Xuzhou 221116, China. 2.—e-mail: xqgu@cumt.edu.cn

Oriented, single-crystal TiO_2 nanorod arrays (NRAs) were synthesized for photoelectrochemical (PEC) water-splitting by a facile hydrothermal route. It was observed that a 500°C annealing process facilitated enhancing the PEC activity of TiO_2 NRAs, in agreement with our previous reports on NRA-related solar cells. Further, electrochemical impedance measurements were employed to investigate the underlying mechanism. Compared with pristine TiO_2 NRAs, the 500°C sintered samples showed a positive flat-band shifting of ~0.12 V as well as a suppression of the donor density. Thus, suggesting that the enhanced PEC performance might be attributed to the widening of depletion layer regions due to the reduction of crystal defects after sintering. The mechanism was also expanded to explain why the dye-sensitized solar cells made with sintered TiO_2 NRAs exhibited an 11-times higher power conversion efficiency than those consisting of pristine arrays.

Key words: Annealing, photoelectrochemical, TiO_2, nanorod array, Mott–Schottky

INTRODUCTION

Recently, one-dimensional (1D), highly ordered TiO_2 nanostructures have received worldwide attention due to their unique advantages of enhanced charge collection, efficient electrolyte penetration and incident-light harvesting.[1–3] Those 1D structures mainly consisted of polycrystalline TiO_2 nanotube arrays (NTAs),[4] anatase TiO_2 nanorod arrays (NRAs)[5] and single-crystalline rutile TiO_2 NRAs.[6] During them, single-crystalline rutile TiO_2 NRAs directly grown on transparent substrates were the most promising for photoelectrochemical (PEC) applications such as dye-sensitized solar cells (DSSCs),[7] perovskite solar cells,[8] water splitting,[9] pollution removal,[10] and so on. It was generally accepted that the electron diffusion length of rutile TiO_2 NRAs was about five times larger than that of porous nanoparticle (NP) films.[11] In other words, given the same thickness, the DSSCs made with NRA photoanodes were expected to exhibit much higher power conversion efficiencies (PCEs) than the conventional cells using porous NP films.

Early in 2008, Liu and his coworkers reported on the synthesis of TiO_2 NRAs on fluorine-doped tin oxide (FTO) glass via a facile hydrothermal approach, where a PCE of over 3% was demonstrated after being treated by $TiCl_4$.[12] Almost at the same time, Feng et al. also developed a solvothermal route to prepare the ordered, compact TiO_2 NRAs on FTO substrates and obtained a higher PCE of 5%.[13] However, for a considerably long time, the corresponding PCEs were still less than 6% until recently, which mainly resulted from the limited internal surface area (only 3.6–9.7 m^2/g), poor dye loading and, thereby, insufficient light absorption in comparison with mesoporous NP films.[14] It was not likely to obtain a loose, high aspect ratio TiO_2 NRA by increasing the reaction duration, precursor concentration or cyclic times simply, which were demonstrated to be efficient for synthesis of ZnO

(Received May 1, 2015; accepted October 22, 2015; published online November 6, 2015)

NRAs with high surface areas.[15,16] Fortunately, such an issue had been solved by Lv's group in a recent report.[7] They obtained a record efficiency of ~7.91% in DSSCs using TiO_2 NRAs with a thickness of 30 μm. In addition, there were other methods to enhance the PEC activity of TiO_2 NRAs, such as doping with traditional metal elements, surface modification, or annealing.[9,17,18] For instance, in our previous reports, the significantly enhanced PCE (~450%) of DSSCs was realized by simply sintering TiO_2 NRAs in air at 500°C.[18,19] Such a behavior was attributed to the better electric contact and adhesion between the NRAs and substrates. Despite those causes, the reason might be not comprehensive. Were there other factors leading to such an enhancement? It still remains unclear, and few studies have been made to reveal the mechanism, to the best of our knowledge.

In this report, a series of PEC approaches including the electrochemical impedance spectroscopy (EIS) and linear sweep voltammetry (LSV) curves were employed to examine the mechanism underlying the above behavior. As a result, a few carrier transport parameters (especially flat-band potential, electron density and depletion layer thickness) were estimated or calculated from those data. It was found that the annealing treatment facilitated reduction of the electron density as well as widening the depletion region in single nanorods (NRs), which possibly contributed to the enhancement of PEC activities or energy conversion efficiencies of TiO_2 NRAs.

EXPERIMENTAL DETAILS

Synthesis and Sintering of TiO_2 NRAs

Oriented single-crystal TiO_2 NRAs were synthesized on the FTO substrates by a facile hydrothermal method as reported previously.[12] Briefly, the clean FTO substrates were placed in a sealed autoclave (60 mL volume) with the conducting side facing up, containing 0.6 mL of tetrabutyl titanate, 15 mL of hydrochloric acid (HCl, 37 wt.%) and 15 mL of deionized (DI) water. The synthesis process was carried out at 150°C for 8 h. Afterwards, one of them was calcinated in air at 500°C for 30 min, while the other one, without any heat treatment, was used as a reference.

Characterization

X-ray diffraction (XRD) was carried out to characterize the phase structure of the TiO_2 NR arrays on a D8 Advance Bruker diffractometer with Cu Kα irradiation. The morphology and structure were characterized by a field emission scanning electron microscopy (FESEM, S-4800, Hitachi, Japan), and high resolution transmission electron microscopy (HRTEM, JEOL-2010).

PEC Measurements

PEC measurements were performed in a typical three-electrode cell connected to a CHI 660D electrochemical workstation (Shanghai Chenhua). Herein, TiO_2 NRA samples were used as the working electrodes (~1 cm^2), Pt foil as a counter electrode, a saturated calomel [$Hg/HgCl_2$, single-crystal electrode (SCE)] electrode as a reference electrode and 0.05 M Na_2SO_4 aqueous solution as the electrolyte. A 500-W Xe lamp (Beijing Trusttech) was used with an irradiation intensity of 100 mW/cm^2. No optical filter was used, thus the Xe lamp provided full-range light from the ultraviolet (UV) to visible band. Thus, the TiO_2 electrodes could be excited by the irradiation and produced the current output. The current density versus potential (J–V) curve of the working electrode was obtained by the LSV at a scan rate of 50 mV/s. EIS was conducted using with an alternating current signal (10 mV) in the frequency range of 0.1–10^5 Hz at open circuit potential (OCP) under visible-light irradiation. Mott–Schottky (M–S) plots were measured at a frequency of 1 kHz in the dark. All the measurements under irradiation were performed with backside illumination.

RESULTS AND DISCUSSIONS

Through our previous studies,[18–21] no obvious differences were observed in the morphologies, microstructures and phase structures of the pristine and sintered TiO_2 NRAs through XRD, SEM and TEM analysis (Please see Figs. S1, S2, and S3 in Support Information). The single TiO_2 NRs with diameters of 150–200 nm were actually consisted of many secondary NRs with sizes of 20 nm or thinner in thickness.

LSV Curves Under Irradiation

Figure 1 displayed the LSV curves of the pristine and 500°C sintered TiO_2 NRA samples under irradiation. As could be seen, the photocurrent was observed in both the samples from the excitation of UV light (with energy over 3.0 eV). The bumps were observed in two LSV curves at around 0 V, which might be associated with the water splitting. It was noteworthy that the sintered TiO_2 electrode exhibited a much higher photocurrent than the pristine one. The former exhibited a current density of ~0.965 mA/cm^2 at the applied potential of 0.7 V versus the SCE, which was about 20-fold larger than the latter one (just 0.047 mA/cm^2 at the same potential). Besides, the onset potential of the sintered one was approximately −0.552 V, which was more positive than the value (−0.643 V) of the pristine one. Herein, the onset potential corresponded to the state when the photocurrent was reduced to zero, which was also called the open-circuit potential. The above results implied that the band bending necessary for separation of photo-

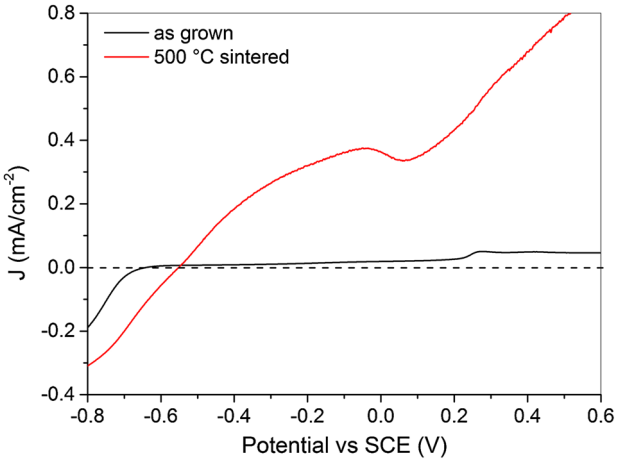

Fig. 1. LSV plots of TiO_2 NRA electrodes under an irradiation intensity of 100 mW/cm^2 (Color figure online).

generated electrons and holes was smaller in the sintered electrodes, in terms of Ref. 22. Further, the enhanced photocurrent might be due to the suppressed charge recombination inside TiO_2 NRAs.

Time Dependence of Photocurrent and Open-Circuit Potential

To examine the photocurrent response, amperometric J–t curves were measured with light on/off cycles at a 0.7 V bias, as indicated in Fig. 2. As seen, the sintered sample showed a much higher photocurrent than the pristine one, in agreement with the LSV results in Fig. 1. From the plot of the sintered electrode, not only a good sensitivity but also a rapid decrease of photocurrent were observed simultaneously just after turning on the light, which was possibly due to the carrier recombination process. Evidently, the higher the photocurrent, the more photo-generated carriers were located inside the electrodes per unit time, resulting in a decay of current soon after the light was turned on. Further, the actual conversion efficiency of a sintered TiO_2 NRA was calculated to be 0.38% by using the following well-known equation[23]:

$$\eta\% = J(1.23 - V)/P \times 100, \qquad (1)$$

where J is the current density under irradiation, V is the applied voltage versus reversible hydrogen electrode (RHE), and P is the input light power intensity of 100 mW/cm^2. Herein, the RHE potential could be deduced from the SCE reference electrode by the relation: $E_{RHE} = E_{SCE} + 0.24\ V + 0.59\ pH$. It suggested that the rutile TiO_2 NRAs still exhibited a response to the sunlight despite a relatively wide band gap of ~3.0 eV.

The open-circuit potential (OCP) curves of two TiO_2 samples under illumination were compared in Fig. 3. The electrode which underwent sintering showed not only a higher OCP value but also a longer electron lifetime τ than the pristine one, similar with the behavior reported in TiO_2-SnO_2 nanotube (NT) electrodes.[24] As a result, it suggested that the annealing treatment favored lengthening the lifetime of photo-generated electrons, in accordance with J–t curves. Moreover, it was also found that the OCP value (before the light was off) was still rising for the pristine sample while it was flat for the sintered sample. That behavior might be associated with the presence of electron accumulation at the NR surface under open-circuit conditions.[25] As a result, it became more difficult to derive away the photo-excited electrons from the TiO_2/electrolyte interfaces, leading to a slower rate researching the saturation current density.

EIS Results

Electrochemical impedance measurements were performed in the dark for collecting M–S plots, and under irradiation for Nyquist plots. Figure 4 displayed the Nyquist plots of the photoelectrodes measured under irradiation and at the OCP over a range of 0.1 Hz to 100 kHz with an alternating current (AC) perturbation of 10 mV. Two semicircles could be identified, of which the small semicircle over the high-frequency range was ascribed to the charge transfer process in the semiconductor depletion layer while the low-frequency arc results from the charge transfer in the Helmholtz layer.[14] Apparently, there wasn't any difference in the small semicircles of the two samples, while the sintered one exhibited a larger diameter for the large semicircles. To achieve the specific information, the Nyquist plots were fitted with an equivalent circuit (inset of Fig. 4) and the fitting results are indicated in Table I. It was clearly seen that there weren't obvious changes in the series resistance (R_1) and the depletion layer resistance (R_2) except a slight increase of the transferring resistance (R_3) at the electrode/solution interface after sintering. The enhanced R_3 might be associated with the poorer band bending of the sintered one, as would be discussed latter.

Figure 5 displayed the M–S ($1/C^2$ versus V) plots of rutile TiO_2 electrodes which were transited from the impedance versus potential (Z–V) curves measured at a constant frequency of 1 kHz and in the dark. As could be seen, the positive slope of the M–S plot indicated the presence of a typical n-type semiconductor characteristic with electrons as the majority carriers. It was also known that the correlation between depletion layer capacitance (C) and applied potential (V) could be described by the following equation[26]:

$$\frac{1}{C^2} = \frac{2}{e_0 \varepsilon \varepsilon_0 N_d}\left[(V - V_{FB}) - \frac{kT}{e_0}\right], \qquad (2)$$

where e_0 is the electron charge, ε is the dielectric constant, ε_0 is the permittivity of a vacuum, N_d is the donor density, V is the applied potential, V_{fb} is the flat-band potential, and kT/e_0 is a temperature-

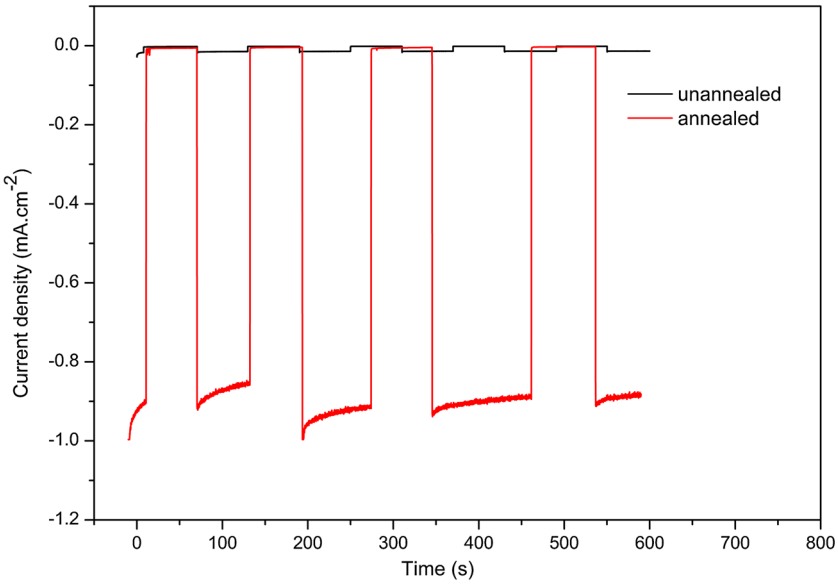

Fig. 2. Photocurrent response versus time at a 0.7 V bias (versus SCE) of TiO_2 NRA electrodes under an irradiation intensity of 100 mW/cm^2 (Color figure online).

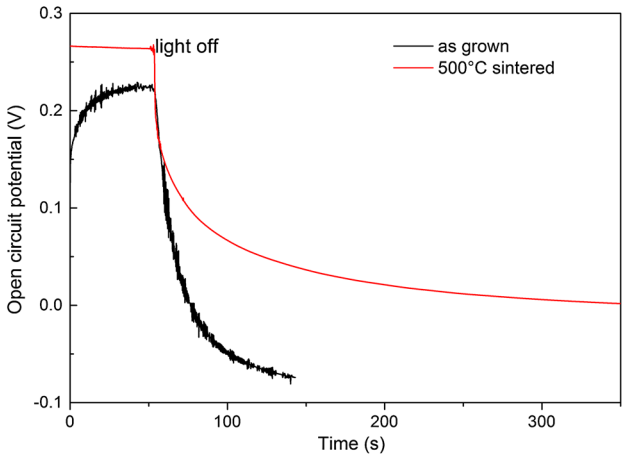

Fig. 3. Transient photovoltage decay curves of TiO_2 NRA electrodes under an irradiation intensity of 100 mW/cm^2 (Color figure online).

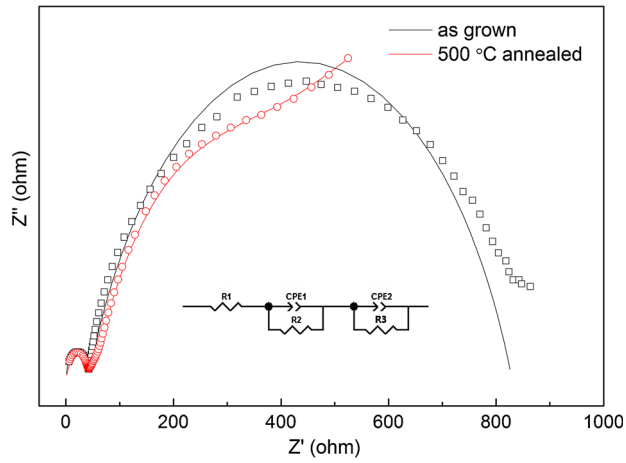

Fig. 4. Nyquist plots of TiO_2 NRA electrodes at −0.7 V (versus an SCE) under irradiation (100 mW/cm^2). Inset: equivalent circuit used to fit the data. Fitting plots are shown as solid lines (Color figure online).

dependent correction term. Naturally, the N_d and V_{fb} could be derived through fitting the linear part of the plots (see Fig. 5), and the fitted results were indicated in Table I. As a result, the sintered TiO_2 NRAs exhibited a lower N_d (1.1×10^{18}/cm^3) as well as a more positive V_{fb} (−0.74 V) than the pristine one. The lower N_d value could be explained by the reduction of crystal defects existing in the grain boundaries of the adjacent secondary NRs. It was demonstrated by the SEM and TEM images and other reports[7] that the single TiO_2 NRs actually consisted of many ultra-thin secondary NRs. The sintering process facilitated the agglomeration of the adjacent NRs. On the other side, the variation of V_{fb} in TiO_2 NRAs was coincident with that of onset potential. Otherwise, the difference between them (V_{fb} and OCP) was so small (~0.2 V for both the samples) that it didn't take a large over-potential to yield a photocurrent. With reference to the pristine electrode, the shifting of V_{fb} towards the positive side implied a weaker band bending occurring near the surface region, being consistent with the lower Fermi level or less donor density. Specifically, the lower the Fermi level, the poorer band bending was near the NR surface, as was illuminated in Fig. 6a and b. According to the Schottky barrier model, the depletion layer width (W) at 0.0 V bia (versus SCE) could be calculated by the equation[17,27,28]:

$$W = \left(\frac{2\varepsilon_0\varepsilon_r\psi}{e^2 N_D}\right)^{1/2}, \qquad (3)$$

where $\psi \equiv E - E_{fb}$ is the maximum potential drop in the depletion layer. A potential of 0.0 V was chosen to calculate the depletion layer because of

the negligible dark current at that potential. The calculated results on the depletion layer widths were indicated in Table II. It was found that the depletion layer thickness of the sintered TiO_2 NRs was ~195 nm, approximately 5 times higher than the pristine one. Taking into account the limited NR diameters (150–200 nm), the sintered NRs were depleted completely with a W value of 75–100 nm, while only the surface region (40 nm) of the pristine one was depleted. The former still possesses a 2–2.5 times higher W value than the latter one. Otherwise, the widened W value could be easily understood in terms of semiconductor theories.[29] The W is in inverse proportion to the N_d, thus, a lower electron density implies a wider depletion layer when the electrolyte remains the same.

Table I. Simulated data from from EIS spectra (Nyquist plots) on the charge transferring resistances under an irradiation intensity of 100 mW/cm^2

Sample	R_1/Ω	R_2/Ω	R_3/Ω
Pristine	1.1	41.8	785
500°C annealed	0.7	41.4	843

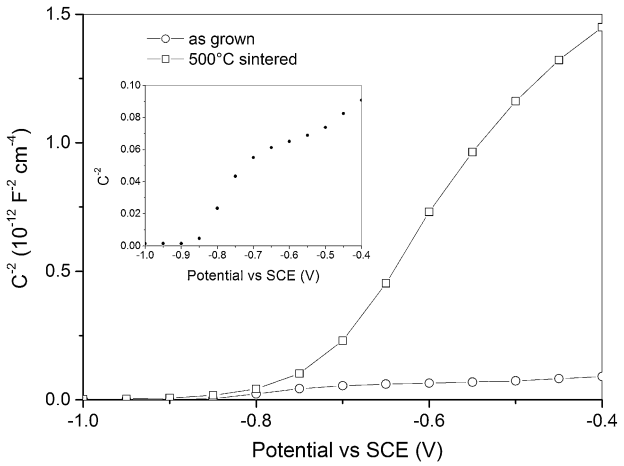

Fig. 5. M–S plots of TiO_2 NRA electrodes at 0.0 V (versus SCE) obtained in the dark. Inset: magnified plot of pristine TiO_2 NRA electrode to display the values of V_{fb} and slope more clearly.

Possible Mechanism

As a result, a schematic model was summarized to explain the real reason that resulted in the enhanced PEC performance of TiO_2 NRA electrodes after annealing, as shown in Fig. 6. Aside from a few factors, such as the enhanced adhesion of NRAs on the substrate which was summarized in our previous reports,[18,19] the main reason might be the widening of depletion layer regions inside the NRs, which is illustrated by Fig. 6a and b. As seen, compared to the pristine TiO_2 electrode, the depletion region width (W) of the sintered one is significantly larger, although the band bending is smaller at the TiO_2/electrolyte interfaces. It is known that the PEC performance of a semiconductor electrode depends on two factors: the degree of band bending and the width of the depletion region. The carriers generated inside the depletion region encounter fewer collisions and lower recombination rates, thus, they can be collected by the FTO electrode with a higher efficiency. As indicated in Fig. 6c, the sintered TiO_2 NRs are depleted completely while the pristine ones are just depleted partly (focused on the surfaces). Thereby, a larger number of the photogenerated carriers are expected to be collected

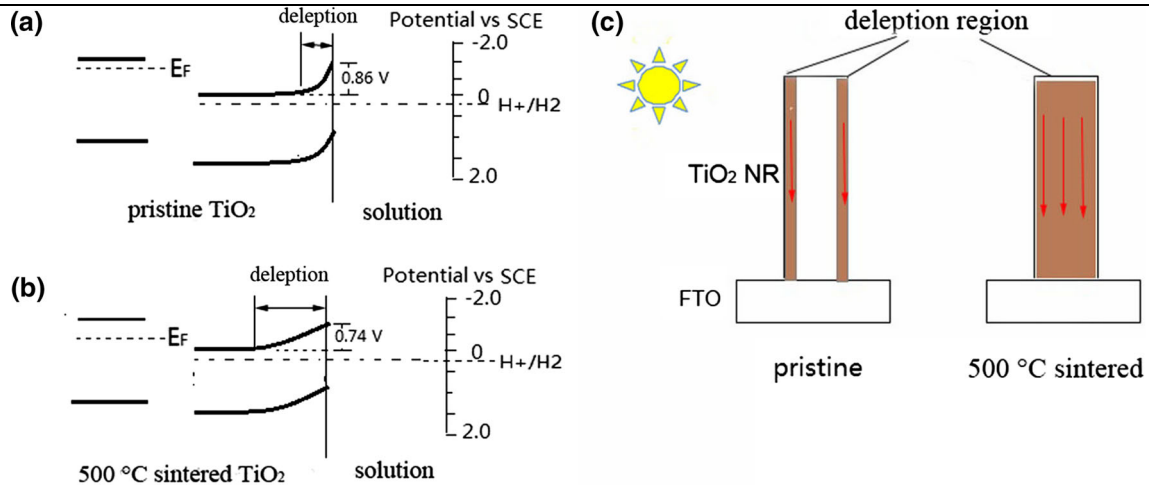

Fig. 6. Energy level diagram of pristine (a) and sintered (b) TiO_2 NRA electrodes. (c) Schematic diagram of the electron transport process inside NRs under irradiation (Color figure online).

Table II. Calculated electronic parameters from M–S plots in the dark

Sample	Slope $k/10^9$	Flat band potential V_{fb} versus SCE/V	Electron density $N_D/10^{18}$ cm^{-3}	Width of depletion W/nm
Pristine	0.4	−0.86 V	14.1	40
500°C sintered	5.0	−0.74 V	1.1	195 (in theory) 75–100 (reality)

by the FTO layers of the sintered samples, leading to an enhancement in PEC performance.

CONCLUSION

Significantly enhanced PEC performance was observed in the single-crystal TiO_2 NRAs after annealing in air at 500°C. Then, a series of approaches including EIS, M-S plots and OCP curves were employed to explain why the PEC activity was enhanced. A PCE of 0.38% at 0.57 V (versus RHE) was obtained in the sintered NRAs under irradiation, which was 11 times higher than the pristine one. In this study, we not only explained the correlation between the changes of flat-band potentials, background electron densities and band bending, but also revealed the effect of the above factors on the photocurrent or PEC characteristic. In summary, aside from the enhanced adhesion of NRAs on the substrates, the sintering process caused the widening of the depletion regions insides single NRs, leading to enhancement of both the lifetime and transport rate of the photo-generated carriers. The above model also provided more direct evidence on why the DSSCs made with sintered TiO_2 NRAs exhibited a superior performance to those fabricated with the pristine ones.

ACKNOWLEDGEMENTS

This work was supported by Natural Science Foundation of Jiangsu Province (BK20130198).

ELECTRONIC SUPPLEMENTARY MATERIAL

The online version of this article (doi:10.1007/s11664-015-4166-x) contains supplementary material, which is available to authorized users.

REFERENCES

1. O.K. Varghese, M. Paulose, and C.A. Grimes, *Nat. Nanotechnol.* 4, 592 (2009).
2. P. Roy, D. Kim, K. Lee, E. Spiecker, and P. Schmuki, *Nanoscale* 2, 45 (2010).
3. C.J. Lin, W.Y. Yu, and S.H. Chien, *J. Mater. Chem.* 20, 1073 (2010).
4. G.K. Mor, K. Shankar, M. Paulose, O.K. Varghese, and C.A. Grimes, *Nano Lett.* 6, 215 (2006).
5. B. Liu, J.E. Boercker, and E.S. Aydil, *Nanotechnology* 19, 505604 (2008).
6. H.E. Wang, Z. Chen, Y.H. Leung, C. Luan, C. Liu, Y. Tang, C. Yan, W. Zhang, J.A. Zapien, I. Bello, and S.T. Lee, *Appl. Phys. Lett.* 96, 263104 (2010).
7. M. Lv, D. Zheng, M. Ye, J. Xiao, W. Guo, Y. Lai, L. Sun, C. Lin, and J. Zuo, *Energy Environ. Sci.* 6, 1615 (2013).
8. D.Y. Son, J.H. Im, H.S. Kim, and N.G. Park, *J. Phys. Chem. C* 118, 16567 (2014).
9. C. Wang, Z. Chen, H. Jin, C. Cao, J. Li, and Z. Mi, *J. Mater. Chem. A* 2, 17820 (2014).
10. Y. Liu, H. Wang, Y. Wang, H. Xu, M. Li, and H. Shen, *Chem. Commun.* 47, 3790 (2011).
11. X. Feng, K. Zhu, A.J. Frank, C.A. Grimes, and T.E. Mallouk, *Angew. Chem. Int. Ed.* 51, 2727 (2012).
12. B. Liu and E.S. Aydil, *J. Am. Chem. Soc.* 131, 3985 (2008).
13. X. Feng, K. Shankar, O.K. Varghese, M. Paulose, T.J. Latempa, and C.A. Grimes, *Nano Lett.* 8, 3781 (2006).
14. X. Wang, Y. Liu, X. Zhou, B. Li, H. Wang, W. Zhao, H. Huang, C. Liang, X. Yu, Z. Liu, and H. Shen, *J. Mater. Chem.* 22, 17531 (2012).
15. M. Law, L.E. Greene, J.C. Johnson, R. Saykally, and P. Yang, *Nat. Mater.* 4, 455 (2005).
16. C. Xu, P. Sin, L. Cao, and D. Gao, *J. Phys. Chem. C* 11, 125 (2010).
17. X. Wang, J. Xie, and C.M. Li, *J. Mater. Chem. A* 3, 1235 (2015).
18. Y. Zhao, X. Gu, and Y. Qiang, *Thin Solid Films* 520, 2814 (2012).
19. X.Q. Gu, Y.L. Zhao, and Y.H. Qiang, *J. Mater. Sci. Mater. Electron.* 23, 1373 (2012).
20. B. Wang and X. Gu, *Micronanoelectronic Technol.* 49, 306 (2012).
21. J.J. Zhu, Y.L. Zhao, L. Zhu, X.Q. Gu, and Y.H. Qiang, *Chin. Phys. B* 23, 48104 (2014).
22. Y. Maeda, Y. Morinaga, Y. Tomita, and K. Kobayashi, *Electrochim. Acta* 54, 1757 (2009).
23. Z. Li, W. Luo, M. Zhang, J. Feng, and Z. Zou, *Energy Environ. Sci.* 6, 347 (2013).
24. U.V. Desai, C. Xu, J. Wu, and D. Gao, *J. Phys. Chem. C* 117, 3232 (2013).
25. P.J. Cameron and L.M. Peter, *J. Phys. Chem. B* 107, 14394 (2003).
26. H.P. Maruska and A.K. Ghosh, *Sol. Energy* 20, 443 (1978).
27. C. Fàbrega, D. Monllor-Satoca, S. Ampudia, A. Parra, T. Andreu, and J.R. Morante, *J. Phys. Chem. C* 117, 20517 (2013).
28. Z. Zhang and J.T. Yates Jr, *Chem. Rev.* 112, 5520 (2012).
29. S.J.A. Moniz, S.A. Shevlin, D.J. Martin, Z.X. Guo, and J. Tang, *Energy Environ. Sci.* 8, 731 (2015).